Editors' Suggestion | Featured in Physics

Geometric Scaling Law in Real Neuronal Networks

Xin-Ya Zhang,[1,2] Jack Murdoch Moore,[1,2] Xiaolei Ru,[1,2] and Gang Yan[1,2,3,*]
[1]MOE Key Laboratory of Advanced Micro-Structured Materials, and School of Physical Science and Engineering, Tongji University, Shanghai 200092, People's Republic of China
[2]Shanghai Research Institute for Intelligent Autonomous Systems, National Key Laboratory of Autonomous Intelligent Unmanned Systems, MOE Frontiers Science Center for Intelligent Autonomous Systems, and Shanghai Key Laboratory of Intelligent Autonomous Systems, Tongji University, Shanghai 201210, People's Republic of China
[3]CAS Center for Excellence in Brain Science and Intelligence Technology, Chinese Academy of Sciences, Shanghai 200031, People's Republic of China

(Received 13 March 2024; accepted 16 July 2024; published 23 September 2024)

We investigate the synapse-resolution connectomes of fruit flies across different developmental stages, revealing a consistent scaling law in neuronal connection probability relative to spatial distance. This power-law behavior significantly differs from the exponential distance rule previously observed in coarse-grained brain networks. We demonstrate that the geometric scaling law carries functional significance, aligning with the maximum entropy of information communication and the functional criticality balancing integration and segregation. Perturbing either the empirical probability model's parameters or its type results in the loss of these advantageous properties. Furthermore, we derive an explicit quantitative predictor for neuronal connectivity, incorporating only interneuronal distance and neurons' in and out degrees. Our findings establish a direct link between brain geometry and topology, shedding lights on the understanding of how the brain operates optimally within its confined space.

DOI: 10.1103/PhysRevLett.133.138401

Introduction—The brain is a remarkable example of complexity, with the human brain containing approximately 10^{11} neurons interconnected by around 10^{14} synaptic connections [1–7]. Particularly awe-inspiring is the emergence of a fully functional brain, as it self-organizes without external guidance, hinting at the presence of as-yet-unrecognized organizational rules. To unveil these hidden rules, studies on neuronal networks, or connectomes, have been crucial, leading to the discovery of important structural properties in brains across various species [8–16]. However, a sole focus on structural aspects overlooks the brain's inherent spatial nature, which is both constrained by and capable of exploiting geometry [17–19].

In this Letter, we explore the geometric principles underpinning neuronal networks by leveraging the data of recently mapped synaptic-resolution connectomes of fruit fly *Drosophila* [20–22]. These connectomes are brainwide and of medium size, featuring 10^3 neurons in the larval stage and 10^5 in adulthood. Importantly, they exhibit a substantial degree of complexity in the connection patterns between neurons. Our analysis reveals a distinct power law governing the scaling of interneuronal connection probability with spatial distance, extending across at least 2 orders of magnitude and persisting from *Drosophila*'s larval stage to maturity. Empirical parameters of this power law align with expectations for supporting effective brain function, but deviations quickly degrade these conditions. Thus, the dependence on the spatial distance of neuronal connection probability appears key to achieving the requisite performance in brain.

Geometric scaling law in the fruit fly neuronal networks—We utilize three synaptic-resolution *Drosophila* connectome datasets, specifically those of first instar larva [20], adult hemibrain [21], and adult whole brain [22]. Focusing on the existence of connections between neuron pairs and excluding the small fraction of neurons for which the spatial coordinates of somas are unavailable, our datasets comprise 2515 neurons with 104 169 connections, 16 782 neurons with 2 372 717 connections, and 127 978 neurons with 2 613 129 connections for the three connectomes, respectively. We compute the Euclidean distance d_{ij} between all pairs of neurons i and j based on their three-dimensional position coordinates, regardless of the presence of synapses between them. The connection patterns between the neurons are represented by an adjacency matrix A, where $A_{ij} = 1$ indicates the existence of at least one synapse from neuron j to neuron i, and $A_{ij} = 0$ otherwise. Hence, the count of neuron pairs separated by distance d is given by $n(d) = \sum_{ij} \delta(d_{ij}, d)$, where the distances are logarithmically binned [23] (refer to

*Contact author: gyan@tongji.edu.cn

Supplemental Material [24], Sec. II). Within this count, $n_c(d) = \sum_{i,j} \delta(d_{ij}, d)\delta(A_{ij}, 1)$ pairs are connected, where $\delta(x, y)$ is the Kronecker delta function [i.e., $\delta(x, y) = 1$ if $x = y$, and $\delta(x, y) = 0$ otherwise]. Therefore, the connection probability of neuron pairs separated by distance d is expressed as $p(d) = n_c(d)/n(d)$.

Despite the distinct morphologies exhibited by the three connectomes at various developmental stages [Figs. 1(a)–1(c)], we analyze the histograms of $n(d)$ and $n_c(d)$ [Figs. 1(d)–1(f)], leading to the discovery of a consistent power-law dependence of the connection probability p_{ij} between any pair of neurons i and j on the spatial distance d_{ij} between them,

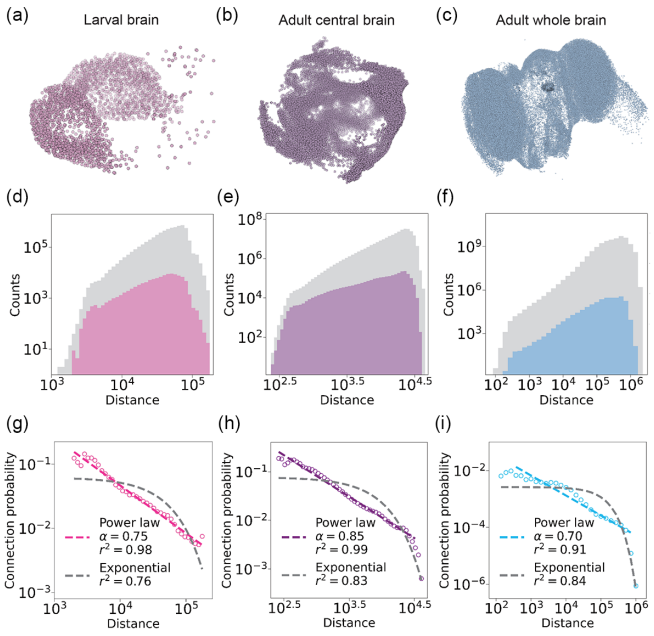

FIG. 1. Geometric scaling law in *Drosophila* connectomes. (a)–(c) The three-dimensional positions of neuron somas in the *Drosophila* larval brain, adult central brain (hemibrain), and adult whole brain, respectively. (d)–(f) Histograms illustrating the Euclidean distances between all neuron pairs [denoted as $n(d)$, depicted in gray] and between connected neuron pairs [denoted as $n_c(d)$, depicted in color]. The unit of distance here is nanometer. Each count represents the number of neuron pairs with distances falling within a specific interval. Logarithmic binning is used. (g)–(i) Each data point represents the connection probability of neuron pairs separated by distance d, calculated as $p(d) = n_c(d)/n(d)$. Best power-law and exponential fits using the least-square regression are denoted by colored and gray dashed lines, respectively, and refer to Fig. S3 in Supplemental Material [24] for the fits using the maximum likelihood estimation. The α values indicate the best-fit power-law exponents, with $\alpha = 0.75$ ($r^2 = 0.98$) for larval brain, $\alpha = 0.85$ ($r^2 = 0.99$) for adult central brain, and $\alpha = 0.70$ ($r^2 = 0.91$) for adult whole brain. Each power-law fit encompasses the range of data points aligned with the corresponding colored dashed line. The coefficient r^2 denotes the regression score R-squared, reflecting the goodness of fit.

$$p_{ij} \propto d_{ij}^{-\alpha}, \tag{1}$$

where $\alpha = 0.75$, 0.85, and 0.70, respectively [Figs. 1(g)–1(i)]. This dependence suggests that connection probability decays with spatial separation following a power law (refer to Supplemental Material [24], Sec. II, for details), representing a notable departure from the exponential distance rule previously observed in the coarse-grained interareal brain networks of various species [38–44] and widely used in brain models [45,46]. While a few generative models of brain networks consider a power-law dependence of interareal connection probability on spatial distance, the exponent is often best-fitted to be larger than 3.0 [47–50], significantly overestimating the strength of geometric constraints on network topology. Taken together, the finding Eq. (1) unveils a novel geometric scaling law, suggesting that there are many more long-range connections at the neuron level compared to macroscopic connectomes. This scaling law holds important implications for the functions of brain networks, as demonstrated below.

Geometric scaling law maximizes information communication—We evaluate the functional implications of the geometric scaling law from two perspectives. The first involves assessing the information communication capacity between neurons, a pivotal function of connectomes that underpins various brain activities [51]. To achieve this, we randomly sample 1000 neurons from the entire connectome of adult *Drosophila* with their soma coordinates in three dimensions and assign them in and out degrees randomly drawn from the empirical distributions. Subsequently, we connect each pair of neurons according to the spatially dependent probability given by Eq. (1), allowing for a tunable power-law exponent α (refer to Supplemental Material [24], Sec. III, for network generation).

We use information entropy [52] to measure the communication capacity between neurons. Specifically, the information brought by a neuron j to a neighbor i can be assessed by considering the neuron set comprised by j and all its neighbors [53]. Therefore, the amount of information collected by i is characterized by the entropy of the entire set $\mathcal{L}_i$ (see Supplemental Material [24], Fig. S11), defined as [53]

$$\phi_i = -\sum_{j=1}^{n} q_j \log q_j. \tag{2}$$

Here, n is the total number of neurons in the network and q_j denotes the frequency of neuron j appearing in the set, i.e., $q_j = \text{count}(j|\mathcal{L}_i)/\text{length}(\mathcal{L}_i)$.

Given that signal propagation between neurons consumes metabolic energy, as indicated by path length [51], we assign each neuron an amount of energetic cost $\bar{k}\,\bar{d}$, where $\bar{k}$ is the average neuronal degree in the empirical connectome, and $\bar{d}$ is the average distance between all pairs

of neurons (regardless of connection). Since $\bar{k}\,\bar{d}$ represents the average energetic cost when neurons are randomly connected, we then investigate the information entropy $\phi = \sum_{i=1}^{n} \phi_i/n$ under this cost constraint, as the exponent α of the power-law dependence varies.

Because the connections between neurons are directional, we calculate both receiving and sending information entropy. As depicted in Fig. 2(a), a narrow range of α values balances the receiving and sending entropy, and interestingly, the empirical α values of the three *Drosophila* connectomes are all within this range. We also consider connections as bidirectional and find that the information entropy reaches the maximum when α is around 0.8 [Fig. 2(b)], close to the three empirical values. The converging results indicate that power-law spatial dependence Eq. (1) optimizes the diversity of information propagating in connectomes, consistently maximizing the communication capacity of *Drosophila* brain.

Geometric scaling law gives rise to functional criticality—Next, we evaluate the functional implications of the geometric scaling law from the perspective of neural activity. For this purpose, on the network of 1000 sampled neurons connected by the power-law spatial dependence described above, we assign each connection a weight randomly drawn from the empirical distribution, and perform simulations of two dynamical models: the Hindmarsh-Rose [54] and the FitzHugh-Nagumo [55] neuronal dynamics (refer to Supplemental Material [24], Sec. IV, for dynamical simulation details). We are particularly interested in examining the influence of spatial dependence on functional segregation and integration [56–58]. Brains exhibit modules, which are densely connected sets of neurons.

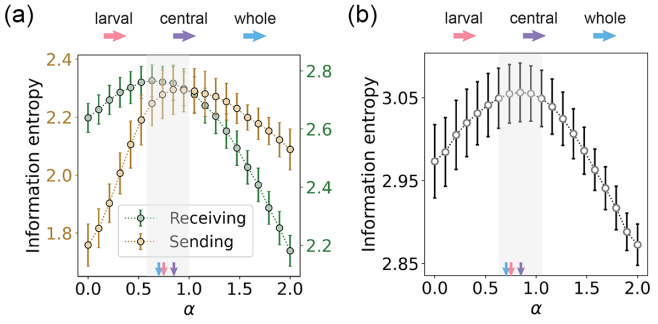

FIG. 2. Geometric scaling law maximizes information entropy of communication across connectome. (a) The sending and receiving information entropy averaged over all neurons versus the varying exponent α, with each neuron assigned an energetic cost of $\bar{k}\,\bar{d}$. The empirical α values of the three connectomes are marked by colored arrows. The shaded region denotes the range centered around the mean of two peaks with a width of 0.4. (b) The average information entropy considering all connections bidirectional versus the varying exponent α. The shaded region denotes the range centered around the peak with a width of 0.4. Error bars represent standard deviation obtained from 1000 independent runs of neuron sampling and network generation.

However, these modules also need to work integrally to coordinate functions globally. Thus, the balance between segregation and integration is crucial for the functioning of brains.

Based on simulated activity of each neuron, we compute the covariance f_{ij} of the temporal activity for any pair of neurons i and j. Subsequently, we quantify the strength of functional segregation and integration using the mean participation coefficient (MPC) metric [44]

$$\mathrm{MPC} = \frac{1}{n}\sum_{i=1}^{n}\left(1 - \sum_{s=1}^{S}\left(\frac{c_{is}}{c_i}\right)^2\right). \tag{3}$$

Here, $c_{is} = \sum_{j\in s} f_{ij}$ is the sum over neuron j in module s, $c_i = \sum_{s=1}^{S} c_{is}$ is the sum of all functional covariance involving neuron i, and S is the total number of structural modules detected using the Louvain's algorithm [59]. Low MPC values indicate functional separation, where neurons mainly engage within their own modules. In contrast, high MPC values imply functional integration, where neurons interact extensively across modules.

As shown in Figs. 3(a) and 3(b), there is a critical transition from high to lower MPC for both dynamical models when varying the exponent α of the power-law spatial dependence. Notably, the empirical α values all fall within the range where the transitions occur, identified by the susceptibility analysis (refer to Fig. S7 in Supplemental Material [24]). This phenomenon remains unchanged when adjusting the excitability parameter and coupling strength of the neuronal dynamics model or setting a fraction of links to be inhibitory (refer to Figs. S12 and S13 in Supplemental Material [24]). We introduce perturbations to the spatial dependence by incorporating an exponential cutoff with coefficient λ into Eq. (1) (refer to Supplemental Material [24], Sec. III). The parameter λ denotes the strength of the exponential cutoff, thus the spatial dependence tends toward an exponential decay with increasing λ. As illustrated in Figs. 3(c) and 3(d), even a small increase in λ abolishes the critical transitions, suggesting that the connectomes rely on a power-law, rather than exponential, geometric constraint to sustain criticality and maintain the functional flexibility of the *Drosophila* brain.

Explicit quantitative predictor for neuronal connectivity—Finally, we are curious about the extent to which spatial dependence shapes neuronal connections. Hence, for each connectome, we randomly sample a substantial number of neuron pairs—half connected and half unconnected. Using the random forest algorithm [60], a machine learning approach, we aim to predict the presence of directional connection from any neuron j to any neuron i based on only five features including spatial distance d_{ij}, in degrees k_i^{in} and k_j^{in}, as well as out degrees k_i^{out} and k_j^{out} [Fig. 4(a)]. The results indicate high prediction accuracy: 81.0% for larva, 83.6% for adult hemibrain, and 96.4% for whole

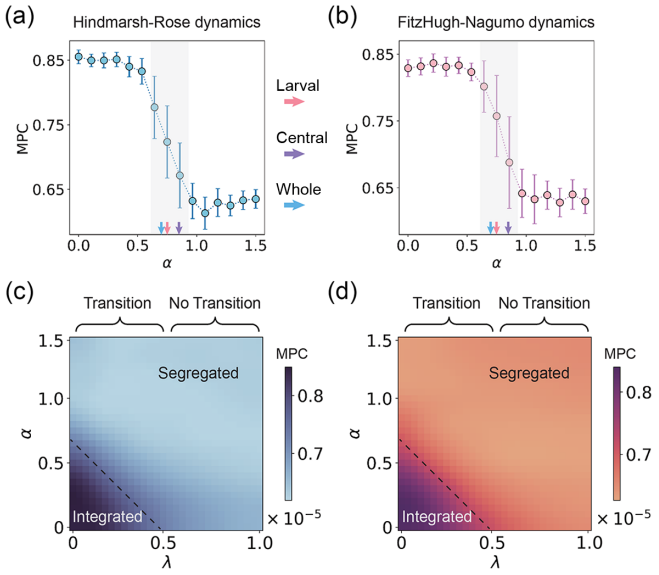

FIG. 3. Geometric scaling law induces functional criticality. (a), (b) Two dynamical models, namely the Hindmarsh-Rose and the FitzHugh-Nagumo neuronal dynamics, are simulated on the 1000-neuron weighted networks. The mean participation coefficient (MPC) is computed from the simulation data of neuronal activity using Eq. (3), where higher MPC values indicate functional integration and lower MPC values indicate functional segregation. Error bars represent the standard deviation obtained from 100 independent runs of network generation and dynamical simulation. The empirical α values of the three connectomes are marked by colored arrows. (c),(d) An exponential cutoff with coefficient λ is introduced into the power-law spatial dependence Eq. (1) to explore changes in MPC for varying α and λ, where λ denotes the strength of the exponential cutoff. The MPC is calculated respectively for the Hindmarsh-Rose (c) and the FitzHugh-Nagumo (d) dynamical models, showing that the critical phase transition from higher to lower MPC disappears when λ is larger than about 0.5×10^{-5}.

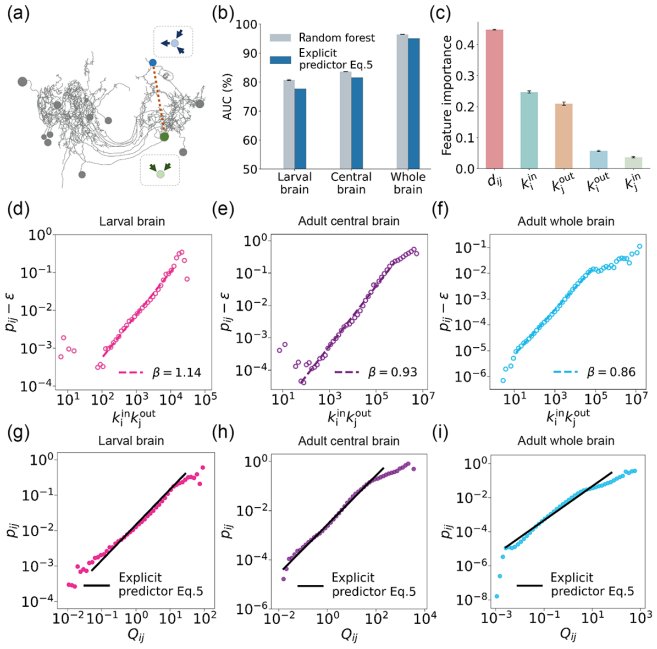

FIG. 4. Explicit quantitative predictor for neuronal connectivity. (a) Five features are used to predict the presence or absence of a directional connection from neuron j to neuron i, including spatial distance d_{ij} (depicted by red dashed line), in degrees k_i^{in} and k_j^{in} (representing the number of incoming connections to each neuron), as well as out degrees k_i^{out} and k_j^{out} (representing the number of outgoing connections from each neuron). (b) Prediction accuracy achieved by the random forest algorithm (81.0%, 83.6%, and 96.4%) and by the explicit quantitative predictor Eq. (5) (77.7%, 81.5%, and 95.1%). The training of the random forest algorithm employs fivefold validation. Accuracy is assessed using the AUC metric (area under the receiver operating characteristic curve). For each connectome, the prediction set comprises all connected neuron pairs and an equivalent number of randomly sampled unconnected neuron pairs, resulting in a random guess accuracy of 50%. (c) Feature importance revealed by the random forest algorithm. (d)–(f) Probability $p_{ij} - \epsilon$ plotted against the product $k_i^{\text{in}} k_j^{\text{out}}$, where ϵ denotes the saturation as described in the main text. Dashed lines indicate the fits of Eq. (4) by least-square regression. Each fit encompasses the range of data points aligned with the corresponding colored dashed line. (g)–(i) The right side of Eq. (5) is abbreviated as Q_{ij}. The dots represent p_{ij} values directly computed from the empirical data of three connectomes. The solid lines represent the explicit quantitative predictor Eq. (5), rather than fitting.

adult connectome [Fig. 4(b)]. Despite the high structural complexity of connectomes, random forest achieves remarkable accuracy, suggesting an underlying simple principle governing connection patterns. This motivates us to further explore for an explicit quantitative predictor of the connection probability between neurons.

When evaluating the likelihood of a connection from neuron j to neuron i, three features—d_{ij}, k_i^{in}, and k_j^{out}—emerge as important [Fig. 4(c)]. Given the discovered spatial dependence in Eq. (1), our attention turns to investigating the impact of k_i^{in} and k_j^{out}. The analysis reveals a relationship captured by

$$p_{ij} - \epsilon \propto (k_i^{\text{in}} k_j^{\text{out}})^{\beta}, \tag{4}$$

where the exponent β equals 1.14, 0.93, and 0.86 for the three connectomes, respectively [Figs. 4(d)–4(f)]. Here, ϵ represents the saturation probability for $k_i^{\text{in}} k_j^{\text{out}} < \bar{k}$, i.e., when the product $k_i^{\text{in}} k_j^{\text{out}}$ is smaller than the average degree $\bar{k}$, the connection probability reaches a saturation level ϵ and ceases to decay further (refer to Fig. S9 in Supplemental Material [24]). It is noteworthy that the three β exponents are all close to 1.0, i.e., a neuron's attraction is approximately proportional to its degree, consistent with observations in many complex networks [61,62].

By combining Eqs. (1) and (4), we derive an explicit quantitative predictor for the likelihood of neuronal connections,

$$p_{ij} \propto [(k_i^{\text{in}} k_j^{\text{out}})^{\beta} + \bar{k}^{\beta}] d_{ij}^{-\alpha}. \quad (5)$$

Detailed derivation is available in Supplemental Material [24], Sec. V. The specific values of the two parameters α and β in Eq. (5) are determined by our analysis above. As shown in Figs. 4(g)–4(i), the quantitative relationship in Eq. (5) agrees well with the empirical data of the three connectomes. Remarkably, when applying the explicit relationship to predict neuronal connectivity, it achieves accuracy comparable to that of the random forest algorithm [Fig. 4(b)].

Discussion—In this Letter we have revealed a consistent scaling law between connection probability and spatial distance in the neuronal networks of fruit fly *Drosophila* across different developmental stages. This power-law decay behavior significantly differs from the exponential distance rule observed in coarse-grained interareal brain networks, highlighting a considerably higher probability of long-range connections between distant neurons than previously thought. By incorporating spatial dependence and considering neurons' degrees, we have derived an explicit quantitative predictor for the neuronal connection pattern. The interpretable predictor does not need intensive training but can achieve comparable accuracy to a black-box machine learning algorithm, emphasizing its effectiveness in capturing the fundamental laws governing *Drosophila* connectomes.

Despite the inherent complexity of connectomes, we have demonstrated that the geometric scaling law alone carries important functional implications. It enables the brain to reach the maximum capacity for information communication and to operate around critical states that balance network integration and separation. These results align with the hypothesis that the brain works at the edge of a critical phase transition between order and disorder [63–68].

Our work raises intriguing questions for future research. First, our analysis considered the presence or absence of connections between neuron pairs. Future studies could extend this analysis to include connection weights, incorporating factors such as the number of synapses [69], which might help resolve discrepancies in the connection-distance relationship at different scales [38–44,70]. Second, while we used Euclidean distance between neuron somas, future research might delve into synaptic morphology, including the length of axons. Third, it is worthwhile to explore the relationship between the connection-distance dependence discovered in this study and the log-dynamics phenomena [71] through more detailed simulations of neuronal activity. Last, a recent study showed that spatially embedded artificial neural networks can generate a variety of architectural and computational features similar to those of real brains [72], hinting at new opportunities for developing brain geometry-inspired artificial intelligence. These endeavors will contribute to a more comprehensive understanding and broader applications of the geometric aspects of brain connectomes.

Acknowledgments—This work was supported by National Natural Science Foundation of China (Grants No. T2225022, No. 12161141016, No. 12350710786, and No. 62088101), STI2030 Major Project (Grant No. 2021ZD0204500), Shanghai Municipal Science and Technology Major Project (Grant No. 2021SHZDZX0100), Shuguang Program of Shanghai Education Development Foundation and Shanghai Municipal Education Commission (Grant No. 22SG21), and the Fundamental Research Funds for the Central Universities. We thank Benjamin D. Pedigo for his help in larval connectome data acquisition, and Eduardo G. Altmann for insights about statistical laws.

Data availability—Our code is provided via https://github.com/xinyacheung/geoscaling.

[1] E. Bullmore and O. Sporns, Complex brain networks: Graph theoretical analysis of structural and functional systems, Nat. Rev. Neurosci. **10**, 186 (2009).
[2] E. Tang and D. S. Bassett, Colloquium: Control of dynamics in brain networks, Rev. Mod. Phys. **90**, 031003 (2018).
[3] C. Presigny and F. DeVicoFallani, Colloquium: Multiscale modeling of brain network organization, Rev. Mod. Phys. **94**, 031002 (2022).
[4] D. L. Barabási *et al.*, Neuroscience needs network science, J. Neurosci. **43**, 5989 (2023).
[5] C. Zhou, L. Zemanová, G. Zamora, C. C. Hilgetag, and J. Kurths, Hierarchical organization unveiled by functional connectivity in complex brain networks, Phys. Rev. Lett. **97**, 238103 (2006).
[6] M. Zheng, A. Allard, P. Hagmann, Y. Alemoán-Gómez, and M. Ángeles Serrano, Geometric renormalization unravels self-similarity of the multiscale human connectome, Proc. Natl. Acad. Sci. U.S.A. **117**, 20244 (2020).
[7] V. Dichio and F. DeVicoFallani, Exploration-exploitation paradigm for networked biological systems, Phys. Rev. Lett. **132**, 098402 (2024).
[8] D. S. Bassett and E. T. Bullmore, Small-world brain networks revisited, The Neuroscientist **23**, 499 (2017).
[9] M. P. Van Den Heuvel and O. Sporns, Rich-club organization of the human connectome, J. Neurosci. **31**, 15775 (2011).
[10] G. Ball *et al.*, Rich-club organization of the newborn human brain, Proc. Natl. Acad. Sci. U.S.A. **111**, 7456 (2014).
[11] O. Sporns and R. Kötter, Motifs in brain networks, PLoS Biol. **2**, e369 (2004).
[12] Y. Wei, X. Liao, C. Yan, Y. He, and M. Xia, Identifying topological motif patterns of human brain functional networks, Hum. Brain Mapp. **38**, 2734 (2017).

[13] Y. N. Kenett, R. F. Betzel, and R. E. Beaty, Community structure of the creative brain at rest, NeuroImage **210**, 116578 (2020).
[14] S. Gu *et al.*, Controllability of structural brain networks, Nat. Commun. **6**, 8414 (2015).
[15] G. Yan, P. E. Vértes, E. K. Towlson, Y. L. Chew, D. S. Walker, W. R. Schafer, and A.-L. Barabási, Network control principles predict neuron function in the caenorhabditis elegans connectome, Nature (London) **550**, 519 (2017).
[16] F. Morone and H. A. Makse, Symmetry group factorization reveals the structure-function relation in the neural connectome of Caenorhabditis elegans, Nat. Commun. **10**, 4961 (2019).
[17] J. A. Roberts, A. Perry, A. R. Lord, G. Roberts, P. B. Mitchell, R. E. Smith, F. Calamante, and M. Breakspear, The contribution of geometry to the human connectome, NeuroImage **124**, 379 (2016).
[18] J. Stiso and D. S. Bassett, Spatial embedding imposes constraints on neuronal network architectures, Trends Cognit. Sci. **22**, 1127 (2018).
[19] J. C. Pang, K. M. Aquino, M. Oldehinkel, P. A. Robinson, B. D. Fulcher, M. Breakspear, and A. Fornito, Geometric constraints on human brain function, Nature (London) **618**, 566 (2023).
[20] M. Winding *et al.*, The connectome of an insect brain, Science **379**, eadd9330 (2023).
[21] L. K. Scheffer *et al.*, A connectome and analysis of the adult drosophila central brain, eLife **9**, e57443 (2020).
[22] S. Dorkenwald *et al.*, Neuronal wiring diagram of an adult brain, bioRxiv, 10.1101/2023.06.27.546656 (2023).
[23] Y. Virkar and A. Clauset, Power-law distributions in binned empirical data, Ann. Appl. Stat. **8**, 89 (2014).
[24] See Supplemental Material at http://link.aps.org/supplemental/10.1103/PhysRevLett.133.138401, which includes Refs. [25–37], for additional information about connectome data, data analysis, network generation, dynamical simulation, theoretical analysis, and connection prediction.
[25] A. Clauset, C. R. Shalizi, and M. E. Newman, Power-law distributions in empirical data, SIAM Rev. **51**, 661 (2009).
[26] A. D. Broido and A. Clauset, Scale-free networks are rare, Nat. Commun. **10**, 1017 (2019).
[27] I. Voitalov, P. vanderHoorn, R. vanderHofstad, and D. Krioukov, Scale-free networks well done, Phys. Rev. Res. **1**, 033034 (2019).
[28] M. Gerlach and E. G. Altmann, Testing statistical laws in complex systems, Phys. Rev. Lett. **122**, 168301 (2019).
[29] J. M. Moore, G. Yan, and E. G. Altmann, Nonparametric power-law surrogates, Phys. Rev. X **12**, 021056 (2022).
[30] Y. Malevergne, V. Pisarenko, and D. Sornette, Testing the Pareto against the lognormal distributions with the uniformly most powerful unbiased test applied to the distribution of cities, Phys. Rev. E **83**, 036111 (2011).
[31] P. Virtanen *et al.*, SciPy1.0: Fundamental algorithms for scientific computing in PYTHON, Nat. Methods **17**, 261 (2020).
[32] M. Storace, D. Linaro, and E. de Lange, The hindmarsh–rose neuron model: Bifurcation analysis and piecewise-linear approximations, Chaos **18**, 033128 (2008).
[33] X. Ru, X.-Y. Zhang, Z. Liu, J. M. Moore, and G. Yan, Attentive transfer entropy to exploit transient emergence of coupling effect, in *Proceedings of the 37th International Conference on Neural Information Processing Systems*, NIPS '23 (Curran Associates Inc., Red Hook, NY, USA, 2024).
[34] M. I. Rabinovich, P. Varona, A. I. Selverston, and H. D. I. Abarbanel, Dynamical principles in neuroscience, Rev. Mod. Phys. **78**, 1213 (2006).
[35] T.-T. Gao and G. Yan, Autonomous inference of complex network dynamics from incomplete and noisy data, Nat. Comput. Sci. **2**, 160 (2022).
[36] E. A. Leicht and M. E. J. Newman, Community structure in directed networks, Phys. Rev. Lett. **100**, 118703 (2008).
[37] F. Pedregosa *et al.*, SCIKIT-LEARN: Machine learning in PYTHON, J. Mach. Learn. Res. **12**, 2825 (2011).
[38] M. Ercsey-Ravasz, N. T. Markov, C. Lamy, D. C. Van Essen, K. Knoblauch, Z. Toroczkai, and H. Kennedy, A predictive network model of cerebral cortical connectivity based on a distance rule, Neuron **80**, 184 (2013).
[39] N. T. Markov, M. Ercsey-Ravasz, D. C. Van Essen, K. Knoblauch, Z. Toroczkai, and H. Kennedy, Cortical high-density counterstream architectures, Science **342**, 1238406 (2013).
[40] S. Horvát *et al.*, Spatial embedding and wiring cost constrain the functional layout of the cortical network of rodents and primates, PLoS Biol. **14**, e1002512 (2016).
[41] G. Deco, Y. S. Perl, P. Vuust, E. Tagliazucchi, H. Kennedy, and M. L. Kringelbach, Rare long-range cortical connections enhance human information processing, Curr. Biol. **31**, 4436 (2021).
[42] X.-J. Wang and H. Kennedy, Brain structure and dynamics across scales: In search of rules, Curr. Opin. Neurobiol. **37**, 92 (2016).
[43] J. A. Roberts, A. Perry, G. Roberts, P. B. Mitchell, and M. Breakspear, Consistency-based thresholding of the human connectome, NeuroImage **145**, 118 (2017).
[44] R. F. Betzel and D. S. Bassett, Specificity and robustness of long-distance connections in weighted, interareal connectomes, Proc. Natl. Acad. Sci. U.S.A. **115**, E4880 (2018).
[45] H. F. Song, H. Kennedy, and X.-J. Wang, Spatial embedding of structural similarity in the cerebral cortex, Proc. Natl. Acad. Sci. U.S.A. **111**, 16580 (2014).
[46] S. Oldham, B. D. Fulcher, K. Aquino, A. Arnatkevičiūtė, C. Paquola, R. Shishegar, and A. Fornito, Modeling spatial, developmental, physiological, and topological constraints on human brain connectivity, Sci. Adv. **8**, eabm6127 (2022).
[47] M. Kaiser and C. C. Hilgetag, Modelling the development of cortical systems networks, Neurocomput. **58**, 297 (2004).
[48] P. E. Vértes, A. F. Alexander-Bloch, N. Gogtay, J. N. Giedd, J. L. Rapoport, and E. T. Bullmore, Simple models of human brain functional networks, Proc. Natl. Acad. Sci. U.S.A. **109**, 5868 (2012).
[49] R. F. Betzel *et al.*, Generative models of the human connectome, NeuroImage **124**, 1054 (2016).
[50] Y. Liu, C. Seguin, S. Mansour, S. Oldham, R. Betzel, M. A. Di Biase, and A. Zalesky, Parameter estimation for connectome generative models: Accuracy, reliability, and a

fast parameter fitting method, NeuroImage **270**, 119962 (2023).
[51] C. Seguin, O. Sporns, and A. Zalesky, Brain network communication: Concepts, models and applications, Nat. Rev. Neurosci. **24**, 557 (2023).
[52] T. M. Cover and J. A. Thomas, *Elements of Information Theory* (John Wiley & Sons Inc., Hoboken, New Jersey, USA, 2005).
[53] Y. Hu, Y. Wang, D. Li, S. Havlin, and Z. Di, Possible origin of efficient navigation in small worlds, Phys. Rev. Lett. **106**, 108701 (2011).
[54] J. L. Hindmarsh and R. Rose, A model of neuronal bursting using three coupled first order differential equations, Proc. R. Soc. B. Biol. Sci. **221**, 87 (1984).
[55] R. FitzHugh, Impulses and physiological states in theoretical models of nerve membrane, Biophys. J. **1**, 445 (1961).
[56] M. A. Bertolero, B. T. Yeo, and M. D'Esposito, The modular and integrative functional architecture of the human brain, Proc. Natl. Acad. Sci. U.S.A. **112**, E6798 (2015).
[57] Y. Chen, S. Wang, C. C. Hilgetag, and C. Zhou, Features of spatial and functional segregation and integration of the primate connectome revealed by trade-off between wiring cost and efficiency, PLoS Comput. Biol. **13**, e1005776 (2017).
[58] R. Wang, M. Liu, X. Cheng, Y. Wu, A. Hildebrandt, and C. Zhou, Segregation, integration, and balance of large-scale resting brain networks configure different cognitive abilities, Proc. Natl. Acad. Sci. U.S.A. **118**, e2022288118 (2021).
[59] V. D. Blondel, J.-L. Guillaume, R. Lambiotte, and E. Lefebvre, Fast unfolding of communities in large networks, J. Stat. Mech. (2008) P10008.
[60] L. Breiman, Random forests, Mach. Learn. **45**, 5 (2001).
[61] A.-L. Barabasi, *Network Science* (Cambridge University Press, Cambridge, England, 2016).
[62] M. E. J. Newman, *Networks* (Oxford University Press, Oxford, United Kingdom, 2018).
[63] W. L. Shew and D. Plenz, The functional benefits of criticality in the cortex, The Neuroscientist **19**, 88 (2013).
[64] J. M. Beggs, The criticality hypothesis: How local cortical networks might optimize information processing, Phil. Trans. R. Soc. A **366**, 329 (2008).
[65] A. Haimovici, E. Tagliazucchi, P. Balenzuela, and D. R. Chialvo, Brain organization into resting state networks emerges at criticality on a model of the human connectome, Phys. Rev. Lett. **110**, 178101 (2013).
[66] L. Cocchi, L. L. Gollo, A. Zalesky, and M. Breakspear, Criticality in the brain: A synthesis of neurobiology, models and cognition, Prog. Neurobiol. **158**, 132 (2017).
[67] R. Wang, P. Lin, M. Liu, Y. Wu, T. Zhou, and C. Zhou, Hierarchical connectome modes and critical state jointly maximize human brain functional diversity, Phys. Rev. Lett. **123**, 038301 (2019).
[68] A. J. Fontenele *et al.*, Criticality between cortical states, Phys. Rev. Lett. **122**, 208101 (2019).
[69] C. W. Lynn, C. M. Holmes, and S. E. Palmer, Heavy-tailed neuronal connectivity arises from Hebbian self-organization, Nat. Phys. **20**, 484 (2024).
[70] N. T. Markov *et al.*, A weighted and directed interareal connectivity matrix for macaque cerebral cortex, Cereb. Cortex **24**, 17 (2014).
[71] G. Buzsáki and K. Mizuseki, The log-dynamic brain: How skewed distributions affect network operations, Nat. Rev. Neurosci. **15**, 264 (2014).
[72] J. Achterberg, D. Akarca, D. Strouse, J. Duncan, and D. E. Astle, Spatially embedded recurrent neural networks reveal widespread links between structural and functional neuroscience findings, Nat. Mach. Intell. **5**, 1369 (2023).